ACS APPLIED MATERIALS & INTERFACES

Research Article

Cite This: ACS Appl. Mater. Interfaces 2017, 9, 43665−43673

www.acsami.org

Superior Pseudocapacitive Lithium-Ion Storage in Porous Vanadium Oxides@C Heterostructure Composite

Hong-En Wang,[†,‡,§] Xu Zhao,[‡] Kaili Yin,[†] Yu Li,[†] Lihua Chen,[†] Xiaoyu Yang,[†] Wenjun Zhang,[*,§] Bao-Lian Su,[*,†,∥] and Guozhong Cao[*,‡]

[†]State Key Laboratory of Advanced Technology for Materials Synthesis and Processing, Wuhan University of Technology, Wuhan 430070, China

[‡]Department of Materials Science and Engineering, University of Washington, Seattle 98195, United States

[§]Department of Materials Science and Engineering & Center Of Super-Diamond and Advanced Films (COSDAF), City University of Hong Kong, Hong Kong, China

[∥]Laboratory of Inorganic Materials Chemistry (CMI), University of Namur, 61 rue de Bruxelles, B-5500 Namur, Belgium

Supporting Information

ABSTRACT: Vanadium oxides are promising anode materials for lithium-ion batteries (LIBs) due to their high capacity, good safety, and low cost. However, their practical application has been deferred by the poor rate capability and cycling stability. In this work, we report the designed synthesis of porous V_2O_3/VO_2@carbon heterostructure electrode for high-performance LIBs. The synergic effects of porous nanostructures, phase hybridization with self-building electric field at heterointerface, and conductive carbon implantation effectively enhance the electronic/ionic conduction and buffer the volume variation in the composite material. Electrochemical tests reveal that the composite electrode exhibits high Li-ion storage capacities of 503 and 453 mAh/g at 100 and 500 mA/g, as well as good cycling stability with a retained capacity of 569 mAh/g over 105 cycles at 100 mA/g. In-depth kinetics analysis discloses that pseudocapacitive Li-ion storage process dominates in the composite electrode, which is probably enabled by efficient coupling of the heterostructure components. The strategy of in situ carbon implantation and phase hybridization presented herein may be extended to other electrode materials for rechargeable batteries with superior electrochemical properties.

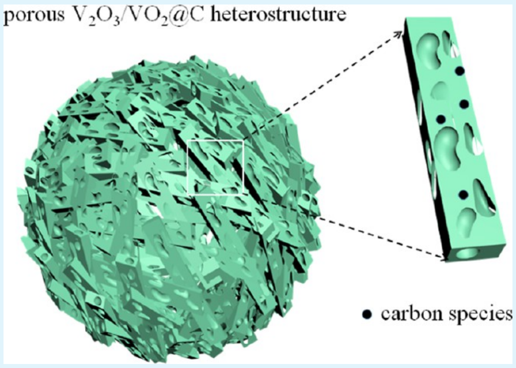

KEYWORDS: *vanadium oxides, heterostructure, lithium-ion batteries, electrodes, pseudocapacitance*

1. INTRODUCTION

Rechargeable Li-ion batteries (LIBs) have been successfully commercialized to power various electronic devices since 1991.[1] Now, they are further improved for emerging use in (hybrid) electric vehicles and smart electric grid, as well as storage of electricity from renewable energies. For this purpose, new cathode and anode materials are being intensively investigated to provide either higher specific energy or better safety, especially both.[2−4]

Graphite and derivatives have been used as anode in commercial LIBs for more than two decades. However, graphite has a relatively low theoretical capacity (372 mAh/g) and a poor rate property. In addition, it is unsafe due to the possible deposition of Li-dendrites on its surface under high charge/discharge rates. Thus, new carbon nanomaterials,[5] nanostructured Si,[6] metal oxide,[7−10] and sulfides/selenides[11−15] have been studied as alternative anode materials for next-generation LIBs. Among them, vanadium oxides possess a rich variety of structural motifs due to their different atomic configurations and multiple valence states of V element.[16,17] The rich composition and phase structures of vanadium oxides have endowed them with superior electrochemical properties as electrodes in LIBs with high theoretical capacities, good safety, and low cost.[18,19] Among them, V_2O_3 and VO_2 have both been explored as promising anode and cathode materials.[20−28] However, as anode, the first discharge process of V_2O_3 and VO_2 usually involves the amorphization of the host structure, and the poor kinetics associated with the energy barrier and cleavage of V−O bonds can lead to a large electrode polarization. Thus, their rate property and cycling stability remain unsatisfactory.

Various low-dimensional V_2O_3 and VO_2 nanostructures have been prepared to enhance their redox reaction kinetics by enlarging the electrode/electrolyte interface and reducing the diffusion paths for Li^+ ions.[29] However, low-dimensional nanomaterials can easily aggregate, possessing a relatively low

Received: September 9, 2017
Accepted: December 1, 2017
Published: December 1, 2017

DOI: 10.1021/acsami.7b13658
ACS Appl. Mater. Interfaces 2017, 9, 43665−43673

packing density with inferior interparticle contact. Hierarchically porous microstructures can effectively improve the particle-packing efficiency and enhance cycling and structure stability. For example, various hierarchically structured porous materials, such as $LiMn_2O_4$,[30,31] TiO_2,[32,33] and V_2O_5,[34,35] have taken full advantage of nanosized building blocks and microsized assemblies, which are beneficial for enhanced strain accommodation and structure integrity. It is anticipated that porous V_2O_3 and VO_2 microstructures with well-defined morphology can manifest excellent Li-ion storage capability.

Coupling vanadium oxides with conductive carbon materials has been proved as another effective strategy to boost their electrochemical properties. For example, Wei et al. reported that V_2O_3-ordered mesoporous carbon composite electrode exhibited a high reversible capacity of 536 mAh/g after 180 cycles at 0.1 A/g.[36] Li et al. prepared a flexible, binder-free anode by encapsulating peapod-like V_2O_3 nanorods into carbon, exhibiting a capacity of 210 and 142.8 mAh/g at 0.1 and 1 C, respectively.[37] In addition, graphene woven VO_2 nanoribbons showed a discharge capacity of 380 mAh/g and 99% capacity retention after 50 cycles.[38] However, most proposed synthetic approaches are still complicated and energy-consuming. Effective syntheses of vanadium oxides/carbon (VO_x@C) hybrids with tailored morphology, composition, and pore structure remain desired and challenging.

Herein, we report the designed synthesis of porous phase-hybridized V_2O_3/VO_2@carbon heterostructure as a novel anode for LIBs. The composite material was obtained by refluxing followed by annealing. The V_2O_3/VO_2 composite electrode features smooth Li^+ ion transfer/intercalation driven by built-in electric field formed at nanosized heterointerfaces. Meantime, in situ carbon incorporation effectively enhances the electrical transport and buffers the volume expansion in the composite electrode during lithiation. The synergic combinations of porous morphology, carbon doping, and presence of interfacial electric field enable fast and stable pseudocapacitive Li-ion storage in the composite electrode as revealed by kinetics analyses. Our work presented herein may pave the way for developing complex metal oxides/sulfides-based composite materials with hybridized phase structures for high-performance LIBs.

2. EXPERIMENTAL SECTION

All of the chemicals were of analytical grade and used as received without further purification.

2.1. Materials Synthesis. Vanadium glycolate (VG) precursors were synthesized by a facile refluxing route. In a typical procedure, 1 mmol ammonium metavanadate (NH_4VO_3) was added into 20 mL ethylene glycol (EG) under stirring. The resulting mixture was heated to 70 °C with continuous stirring to obtain a yellow sol. The sol was then transferred into a 100 mL glass flask and refluxed at 170 °C for 2 h to acquire dark blue VG precipitates. The reaction product was collected by centrifugation, rinsed with absolute ethanol twice, and then dried at 60 °C for 8 h in air.

Hierarchical porous vanadium oxides/carbon (VO_x@C) composites were obtained by annealing the VG precursors at 300−700 °C in Ar with a temperature ramping rate of 2 °C/min. After cooling naturally to room temperature, the samples were collected for following characterization and electrochemical tests. For convenience, the samples annealed at 300, 400, 500, 600, and 700 °C were named as VO_x-300, VO_x-400, VO_x-500, VO_x-600, and VO_x-700, respectively.

2.2. Characterizations. X-ray diffraction (XRD) analyses of the samples were recorded on a Bruker D8 Advanced diffractometer with Cu Kα radiation (λ = 1.54056 Å). Surface morphologies of the samples were observed by a Hitachi S-4800 field-emission scanning electron microscope (SEM) equipped with an energy-dispersive X-ray (EDX) analyzer. Transmission electron microscopy (TEM) and high-resolution transmission electron microscopy (HRTEM) images were acquired using a JEM-2100F transmission electron microscope. Nitrogen adsorption/desorption isotherms were carried out using a NOVA 1200e surface area and pore size analyzer (Quantachrome Instruments) at 77 K. The samples were degassed at 180 °C for 8 h on a vacuum line before adsorption experiments. The specific surface area and pore size distribution of the samples were evaluated by Brunauer−Emmett−Teller (BET) and Barrett−Joyner−Halenda methods. Thermogravimetry (TG) and differential scanning calorimeter (DSC) analyses were recorded using a SETARAM Labsys Evo S60/58458 thermal analyzer under a flow of nitrogen with a heating rate of 5 °C/min. The surface chemical composition and element electronic states were analyzed by an X-ray photoelectron spectroscope (XPS, Thermo Fisher Scientific, Alpha). The binding energy for the sample was calibrated using the C 1s peak from a carbon tape at 284.8 eV.

2.3. Electrochemical Measurements. Electrochemical properties of the samples were tested using CR2025 coin cells. The working electrodes were made by thoroughly mixing the active materials, acetylene black, and poly(vinylidene fluoride) with a weight ratio of 8:1:1 in *N*-methyl-2-pyrrolidone to form a slurry. The slurry was then uniformly coated on a Cu foil and dried at 120 °C for 12 h under vacuum. Li foils were used as counter and reference electrodes. One molar $LiPF_6$ dissolved in ethylene carbonate and dimethyl carbonate with a volume ratio of 1:1 was used as working electrolyte. The Li-half cells were assembled in a glovebox purged with ultrapure Ar. The water and oxygen contents in the glovebox were controlled below 0.5 ppm. Galvanostatic discharge−charge curves were recorded on a LAND CT2001A battery testing instrument within a voltage range of 0.1−3 V versus Li^+/Li at different current densities (50−500 mA/g). Cyclic voltammetry (CV) curves were recorded at different scan rates on a CHI-604E workstation within 0.1−3 V versus Li^+/Li. All of the electrochemical measurements were carried out at room temperature.

3. RESULTS AND DISCUSSION

The porous V_2O_3/VO_2@carbon was synthesized by refluxing NH_4VO_3 in ethylene glycol (EG), followed by annealing in Ar. The starting NH_4VO_3 material displays irregular particle morphology, as revealed by the SEM in Figure S1a,b. During the refluxing process, EG served as a solvent and structure-directing agent. It has a strong coordination ability due to its double hydroxyl groups as bidentate ligands. After refluxing, vanadium(IV) glycolates (VGs) was obtained on a large scale.[39,40] SEM image (Figure S1c,d) indicates the VG precursor comprises microspheres with textured surface. The spheres have an average size of ∼2 μm, and each sphere is constructed by nanosized quadrangular prisms. The VG precursor was then converted into vanadium oxides (VO_x) by thermal treatment. During heat treatment, it is deduced that VG precursor converts into VO_2 first; meantime, some conductive carbon species were in situ incorporated into the VO_x by carbonization decomposition of EG moieties. Carbon doping in VO_x is beneficial for electrical conduction and buffer of volume expansion during discharge. In addition, the formation of carbon can prevent the sintering of vanadium oxides crystals under high temperatures, which facilitates fast Li^+-ion insertion/extraction with short diffusion paths. Further increasing the annealing temperature, the resulting VO_2 could either be further reduced by carbon species into V_2O_3 or directly decompose into V_2O_3.

Before annealing, TG/DSC analyses were performed to probe the decomposition process of VG precursor in inert atmosphere. From Figure 1a, the initial weight loss (∼7.3%) before 200 °C can be ascribed to desorption of physically adsorbed H_2O from the particle surface, which is accompanied

DOI: 10.1021/acsami.7b13658
ACS Appl. Mater. Interfaces 2017, 9, 43665−43673

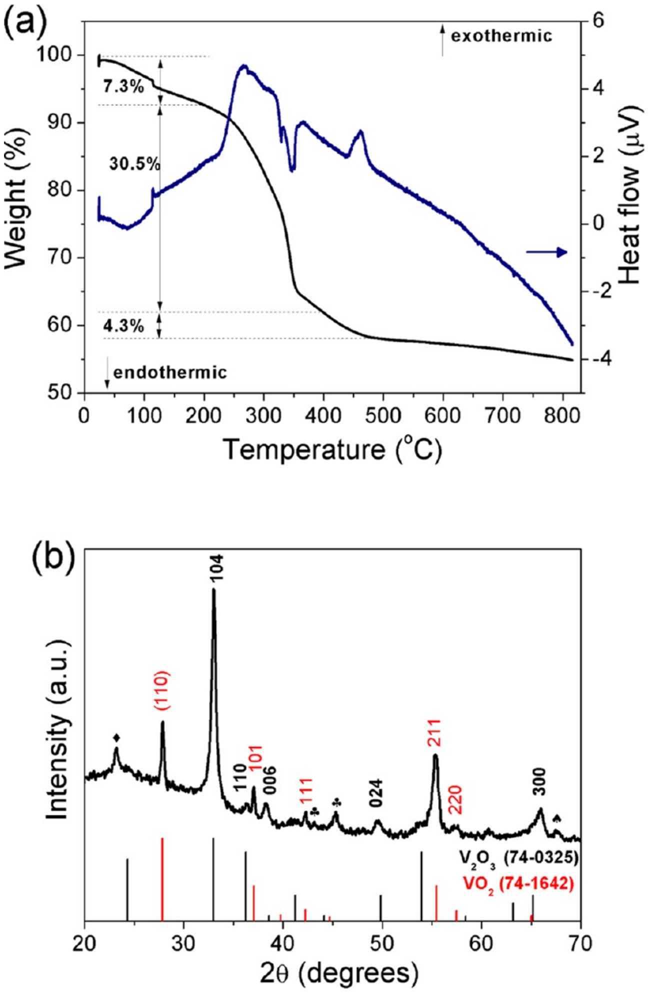

Figure 1. (a) Thermogravimetric analysis (TGA)/DSC curves of VG precursor under N_2 atmosphere with a temperature ramping rate of 5 °C/min; (b) XRD pattern of VO_x-500 sample obtained after annealing the VG precursors at 500 °C for 5 h in Ar. In addition to major V_2O_3 and VO_2 phases, some minor other vanadium oxides of V_6O_{11} (labeled as "♦", JCPDS No. 18-1451), V_3O_5 (labeled as "filled clubs", JCPDS No. 09-0148), and V_3O_7 (labeled as "filled spades", JCPDS No. 27-1347) might also exist in the composite sample.

by an endothermic peak in the DSC curve. A ~30.5% weight loss at 200−400 °C with a noticeable exothermic peak mainly corresponds to the decomposition of EG in the precursor. No crystallographic phases of vanadium oxides were formed before 300 °C, as revealed by XRD pattern (Figure S2a). An endothermic peak is noted at ~345 °C due to the nucleation of VO_2 phase, as confirmed by XRD (Figure S2b). A small weight loss (~4.3%) at 400−500 °C can be attributed to the loss of carbon species together with V_2O_3 phase formation due to the reduction of VO_2 by carbon at high temperature (Figure S2c). From 500 to 700 °C, the weight loss becomes unnoticeable (~1.3%). The combined TG/DSC and XRD results suggest that 500 °C might be optimal for VO_x preparation given the small crystallite size and homogeneous carbonization of EG moieties. Otherwise, an incomplete carbonization can occur at lower temperature (Figure S2a); instead, severe grain growth and aggregation would be expected at higher annealing temperatures (Figure S2d,e). For simplicity, the sample obtained after annealing VG precursor at 500 °C in Ar was named as "VO_x-500", and similar abbreviations were used for other VO_x samples annealed at other temperatures.

Figure 1b depicts the XRD pattern of VO_x-500 sample. The major reflections can be indexed to rhombohedral V_2O_3 phase (JCPDS No. 74-0325)[41] and tetragonal VO_2 (JCPDS No. 74-1642).[42] The coexistence of V_2O_3 and VO_2 phases has several possible advantages: (i) the phase separation can prevent the overgrowth of crystallites into larger-sized single-phase grains; and (ii) abundant nanosized heterojunctions can be formed at the VO_2/V_2O_3 interfaces, which can promote the Li^+/electrons transport/transfer at heterostructure driven by a built-in electric field, as noted recently.[9,11,15,43] Thus, increased Li-ion storage capacity and rate property would be anticipated in such V_2O_3/VO_2 heterostructure electrode. In addition, some minor diffraction peaks are noted and can be assigned to the possible existence of trace V_6O_{11} (JCPDS No. 18-1451), V_3O_5 (JCPDS No. 09-0148), and V_3O_7 (JCPDS No. 27-1347) phases in the composite sample.

SEM image in Figure 2a reveals that VO_x-500 sample contains hierarchical microspheres constructed from quadrangular nanoprisms, which resembles its VG precursor. Magnified SEM image (Figure 2b) indicates that each nanoprism is comprised of nanoparticles interconnected into a porous structure, different from the VG precursor. The porous nanostructure can be produced by the release of gases during thermal decomposition of VG precursors. Apparently, it could facilitate electrolyte permeation and wetting on the electrode surface, and Li^+-ion diffusion with reduced paths, boosting Li-ion storage capability. In addition, EDX mapping discloses uniform element distribution of carbon (C), vanadium (V), and oxygen (O) throughout the sample (Figure 2c−f). This result suggests that some carbon species have been in situ incorporated into VO_x-500 during the thermal decomposition of VG precursor. The mass content of carbon species in VO_x-500 sample was further determined to be ca. 7% by TG/DSC analyses in air (Figure S3). The implantation of carbon species in the sample can enhance the electrical conduction and buffer the volume change of the electrode during charge/discharge, boosting its rate property and cycling stability. For comparison, the morphologies of the VO_x samples obtained after annealing VG precursors at other temperatures were also studied (Figures S4 and S5). For VO_x-300 and VO_x-400 samples, they also comprise microspheres constructed from nanoprism-like particles (Figure S4). However, their surfaces are smooth and only some macropores are formed, suggesting the vanadium oxides grains have been probably buried beneath the thick carbon layer due to the incomplete carbonization of EG at lower temperatures. In contrast, larger-sized V_2O_3 grains (>40 nm) are obtained in VO_x-600 sample possibly due to the overgrowth at higher temperature (Figure S5a,b). Oversized grains (up to 200 nm) together with core/shell microspheres and cracks can be observed in VO_x-700 sample (Figure S5c,d), implying an interparticle sintering by a possible inward−outward Ostwald ripening process. The large grain sizes in VO_x-600 and VO_x-700 samples are disadvantageous for Li^+-ion insertion/extraction, increasing the polarization and lowering the rate capacity.

The microstructure of VO_x-500 sample was studied by TEM/HRTEM. In Figure 3a, the TEM micrograph confirms the well-defined spherical morphology of VO_x-500 particles. Some porous hollow structures of nanoprisms can be observed in Figure 3b,c. HRTEM result (Figure 3d) depicts that the porous nanoprisms are constructed by interconnected nano-

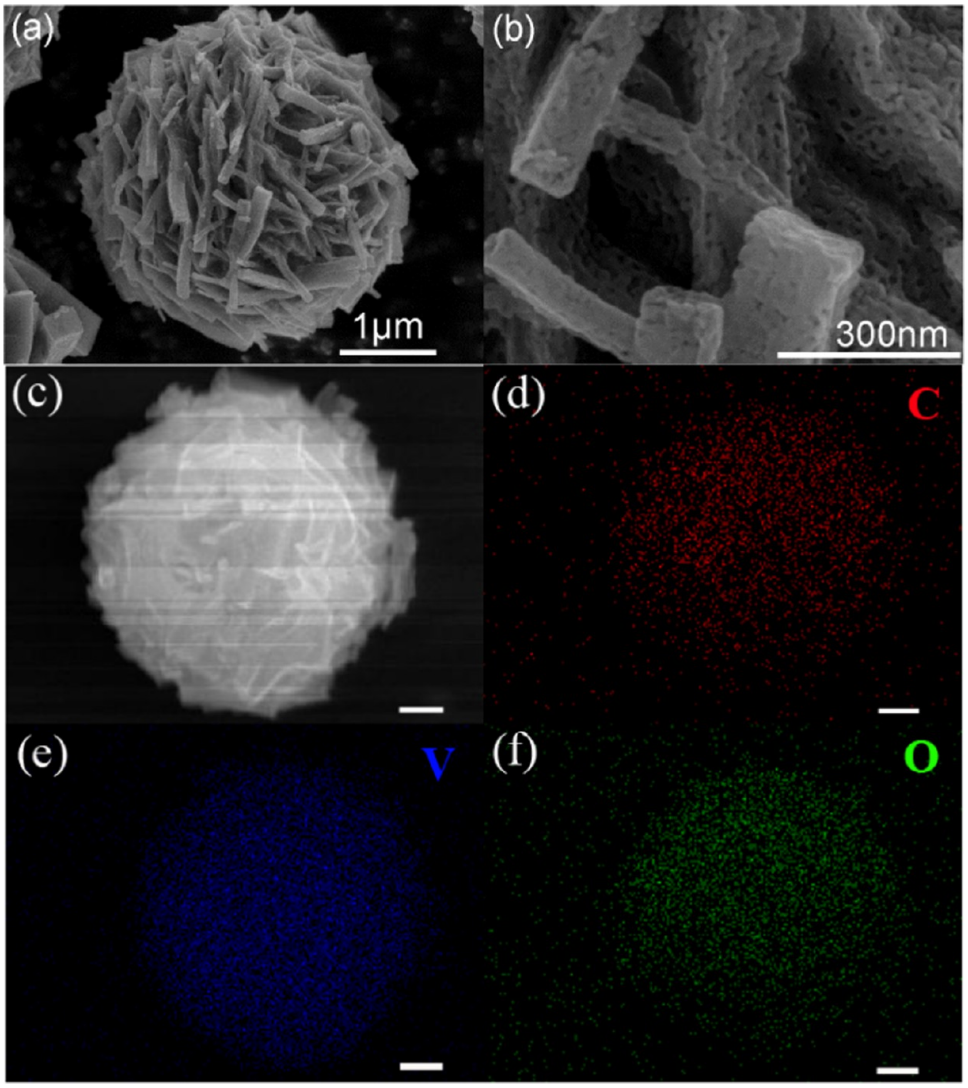

Figure 2. (a, b) SEM images, (c) SEM, and (d−f) corresponding EDX mappings of the C, O, and V distributions in VO_x-500 sample. Scale bars in (c−f) are all 0.5 μm.

particles. The lattice fringes with interplanar distances of 0.37 and 0.32 nm can be indexed to the (012) plane of V_2O_3 and (110) plane of VO_2 phases, respectively.[41,42] In addition, some ultrathin carbon layers can be observed on the outer surface of the vanadium oxides nanocrystals (see arrows). Additional HRTEM micrograph combining fast Fourier transformation (FFT) patterns further confirms the existence of abundant nanosized V_2O_3/VO_2 heterojunctions as shown in Figure 4. The coexistence of V_2O_3 and VO_2 hybridized phases with carbon coating can potentially enhance the Li^+/electron transfer/separation and redox kinetics in the electrode.

The surface element composition and chemical valence states of the elements in VO_x-500 sample were further investigated by XPS analyses (Figure 5). The analysis of V 2p core level XPS spectrum has been combined with O 1s region for accurate peak fitting.[44] As shown in Figure 5a, after deconvolution, the asymmetric shape of V 2p bands can be separated into two sets of valence states. One pair of bands centered at 524.78 and 517.45 eV can be attributed to the spin−orbital splitting components of V $2p_{1/2}$ and V $2p_{3/2}$ in VO_2. The other pair of bands at 523.6 and 516.27 eV can be assigned to the spin−orbital splitting components of V $2p_{1/2}$ and V $2p_{3/2}$ in V_2O_3.[45] The deconvolution of O 1s XPS spectrum reveals three bands at 530.48, 530.86, and 531.82 eV, corresponding to the O−V bond in vanadium oxides,[46] C−O, and C═O bonds,[9] respectively. The high-resolution C 1s XPS spectrum in Figure 5b can be deconvoluted into four bands. The band centered at 284.6 eV can be assigned to the C−C/C═C bonds in amorphous graphite carbon formed during the decomposition of EG species. The band centered at 285.5, 286.5, and 288.3 eV correspond to the C−O, C═O, and O−C═O functional groups of the carbon species, respectively.[36]

Porous nanostructures may possess a large surface area for electrolyte impregnation and mass transport. Nitrogen adsorption/desorption experiments were performed to study the pore structures of VO_x-500 sample. From Figure 6, the sorption isotherms exhibit a type IV curve with a type III hysteresis loop characteristic of mesoporous materials. The sample yields a high BET surface area of ~69.4 m^2/g, which is higher than that of porous V_2O_3/C composite (52.8 m^2/g).[47] The pore size distribution plot (inset in Figure 6) reveals a relatively narrow pore size distribution centering on ~9.8 nm. The relatively high specific surface area of VO_x-500 sample is ascribed to its porous structure with anti-aggregation of

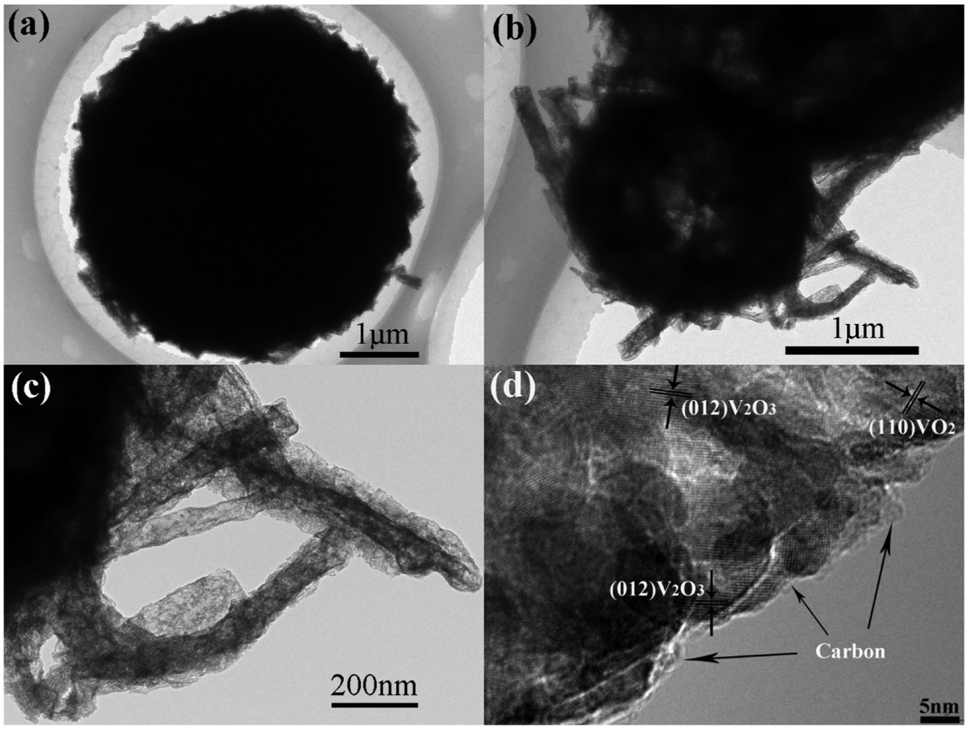

Figure 3. (a−c) TEM images and (d) HRTEM micrograph of VO_x-500 sample containing porous nanoprisms/nanotubes constructed by interconnected V_2O_3 and VO_2 nanoparticles.

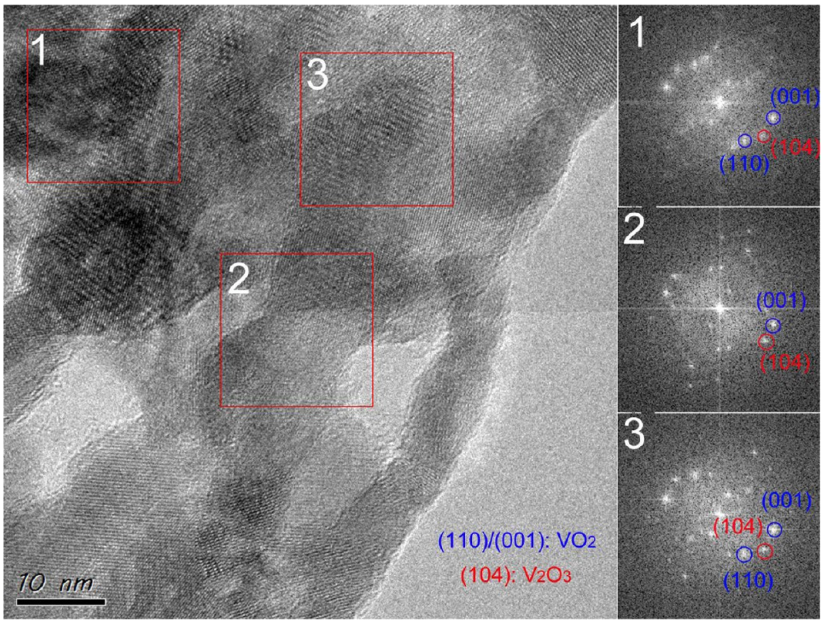

Figure 4. HRTEM micrograph and corresponding FFT patterns of the sample prepared by refluxing following heat treatment in Ar at 500 °C for 5 h (VO_x-500), confirming the presence of abundant nanoscale V_2O_3/VO_2 heterojunctions.

nanoparticles. The high surface area is favorable for Li-ion storage due to the large electrode−electrolyte contact interface with more active sites for Li^+-ion storage, reduced Li^+-ion diffusion path, and accommodation to electrode volume change during repeated (de)lithiation.

The effect of holding time during annealing on the formed hybrid materials was also investigated. Figure S6 depicts the XRD and SEM results of the composite sample obtained by refluxing following heat treatment at 500 °C for 2 h in Ar (denoted as VO_x-500-2). XRD pattern (Figure S6a) reveals that VO_x-500-2 also consists of major V_2O_3 and VO_2 phases and trace V_6O_{11} and V_3O_5 phases. SEM image (Figure S6b) reveals its porous spherical morphology comprising one-dimensional nanobuilding blocks. This result suggests that the phase-hybridized composite can be prepared within a short annealing period as well.

The electrochemical properties of VO_x-500 composite was evaluated using coin-type Li-half cells. For comparison, VO_x-400, VO_x-600 and VO_x-700 samples were also measured under the same conditions. In Figure 7a, the CV curves are displayed

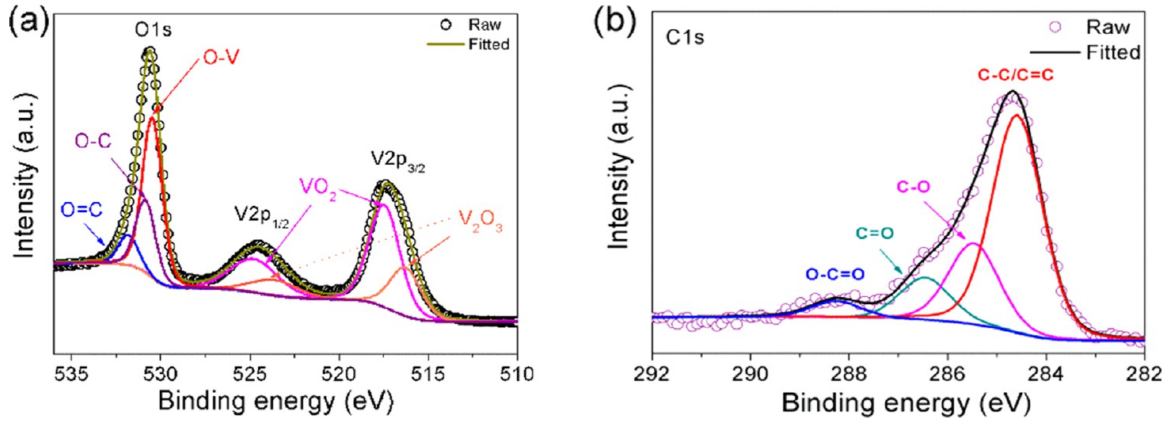

Figure 5. High-resolution XPS spectra of (a) V 2p and O 1s, (b) C 1s in VO_x-500 sample.

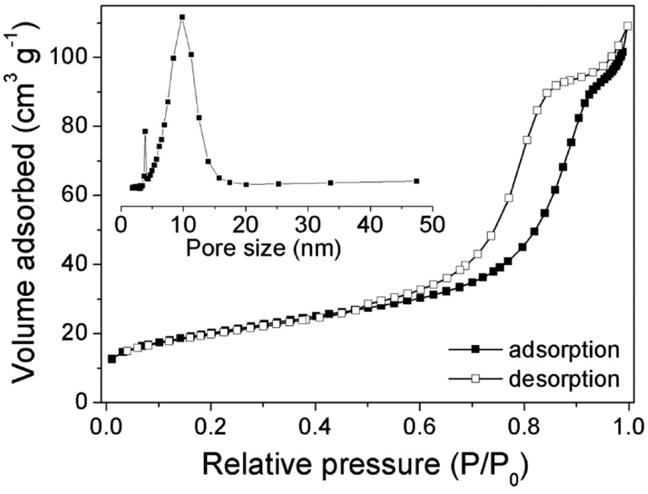

Figure 6. N_2 adsorption/desorption isotherms and pore size distribution plot (inset) of VO_x-500 sample.

to investigate the Li^+-ion insertion/extraction behavior in VO_x-500 electrode. Several pairs of redox peaks can be observed, indicating the multistep redox reactions in the electrode containing hybridized V_2O_3/VO_2 phases. The broad redox peaks at 2.5/2.6 V (peaks A and A′) can be ascribed to the (de)lithiation in VO_2.[48] The redox peaks at 1.7/1.86 V (peaks B and B′) and 1.0/1.2 V (peaks C and C′) correspond to the redox of V^{3+} and V^{4+} in the composite upon Li^+-ion insertion/extraction. Another pair of peaks at 0.5/0.8 V (peaks D and D′) correlate to the partial conversion reactions of V_2O_3/VO_2 into metallic vanadium and Li_2O.[45] The quasi-rectangular shape of the CV curve suggests a capacitor-like Li^+-ion storage behavior. Figure 7b shows galvanostatic discharge/charge curves of VO_x-500 electrode at various current rates. Clearly, VO_x-500 sample displays a high discharge capacity of 860 mAh/g and charge capacity of 534 mAh/g at 50 mA/g, with a Coulombic efficiency of 62.1%. The initial irreversible capacity loss can be mainly ascribed to the electrolyte decomposition accompanied by the formation of a solid−electrolyte interphase layer.[49] Noticeably, VO_x-500 electrode manifests high and stable discharge capacities upon increasing current rates from 100 to 500 mA/g. This fact together with the slopping voltage profiles suggests the Li-ion storage in VO_x-500 may follow a pseudocapacitance-dominant process. Figure 7c depicts the Li-ion storage capability of VO_x-500 electrode at varying current rates. Evidently, VO_x-500 electrode demonstrates a good cycling property with highly reversible capacities of 503, 487, and 453 mAh/g at 100, 200, and 500 mA/g, respectively. From Figure 7d, VO_x-500 electrode shows a Li-ion storage capacity of 523 mAh/g at the third cycle and a retained capacity of 569 mAh/g over 105 cycles. In contrast, all VO_x-400, VO_x-600, and VO_x-700 electrodes exhibit very poor Li-ion storage capacity at 100 mA/g. The Li-ion storage properties of VO_x-500 electrode is also superior or comparable to some V_2O_3 nanostructures reported in the literatures, such as composites of V_2O_3-ordered mesoporous carbon,[36] carbon-coated yolk-shell V_2O_3,[45] and peapod-like V_2O_3 nanorods encapsulated in carbon.[37]

To further understand the kinetics origin, the CV curves of VO_x-500 electrode were recorded at scan rates from 0.1 to 2.0 mV/s, as shown in Figure 8a. The degree of capacitive effect can be analyzed according to the relationship between the measured current (i) and scan rate (v) from the CV curves: $i = av^b$, where "a" and "b" are both constants. The value b is between 0.5 and 1.0, which is determined from the slope of the $\log(i)$ versus $\log(v)$ plot. It is well known that for a diffusion-controlled process, b approaches 0.5, whereas for a surface capacitance-dominated process, b is close to 1.0. In the current experiments, the b values for cathodic and anodic sweep processes are calculated to be 0.79 and 0.95, respectively (inset of Figure 8a). The high b values suggest a more favored capacitive storage kinetics of the electrode. In Figure 8b, the percentage of capacitive contribution to the current at a fixed voltage is further quantitatively determined by separating the current response i from the diffusion-controlled and capacitive contribution at the corresponding voltage. The calculated result unravels that 82% of the total capacity stems from the pseudocapacitive contribution for VO_x-500 electrode, which well explains its superior rate capability.[50] In addition, the rest (∼18%) capacity contribution should mostly stem from the intercalation storage, given the pseudocapacitance mainly involves the surface or subsurface Faradaic process. In the composite anode, the vanadium oxides should contribute most to the total capacity for two reasons. (i) carbon materials derived from common annealing organic/polymer precursors usually exhibited relatively low Li-ion storage capability (e.g., an optimum Li-ion storage capacity of ∼400 mAh/g had been achieved within a voltage region of 0.01−2 V (vs Li^+/Li) at 100 mA/g for porous hard carbon spheres obtained by carbonization of resol resin at 700 °C for 4 h in Ar).[51] (ii) The mass content of carbon in VO_x-500 is estimated to be 7% using TGA in air (Figure S3).

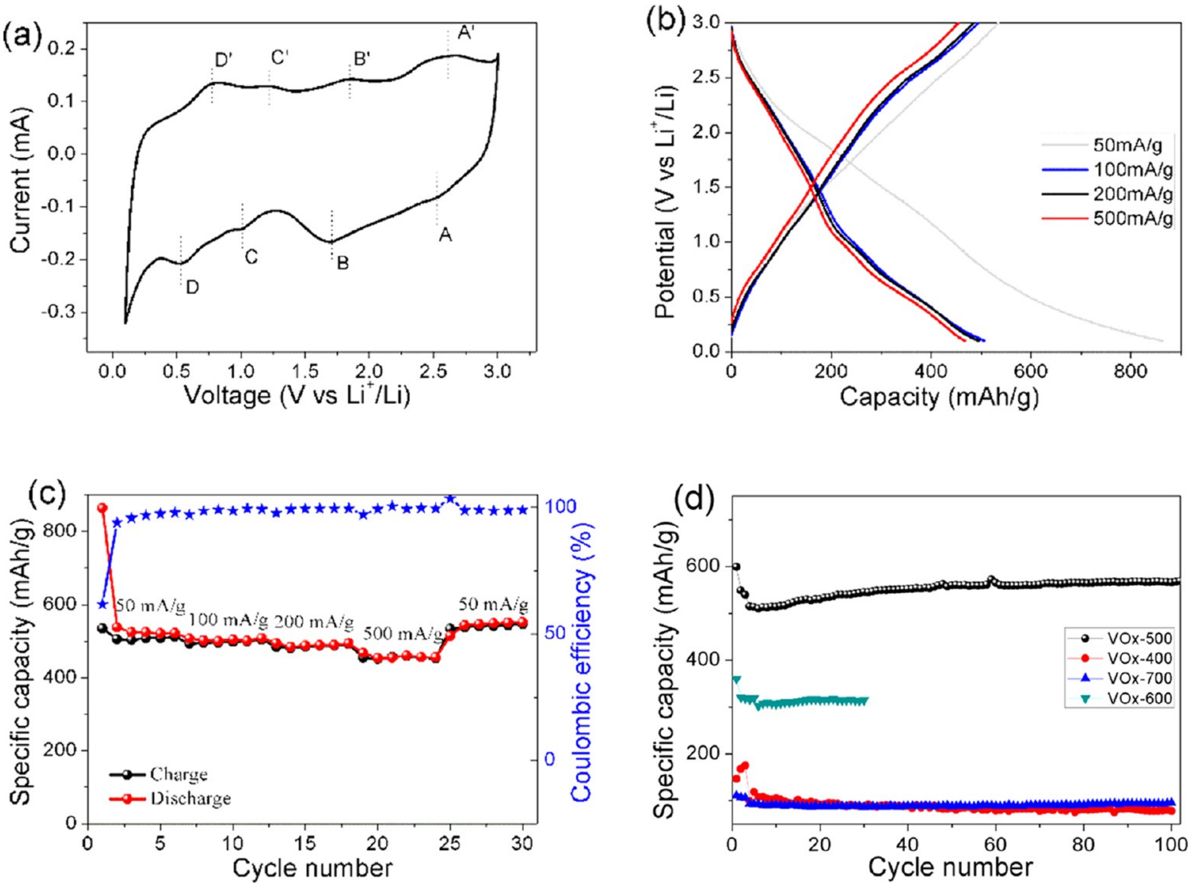

Figure 7. (a) CV curve of VO_x-500 electrode at 0.2 mV/s. (b) Galvanostatic discharge/charge curves of VO_x-500 electrode at different current rates. (c) Rate property of VO_x-500 electrode. (d) Cycling properties of VO_x-500, VO_x-400, VO_x-600, and VO_x-700 electrodes at 100 mA/g.

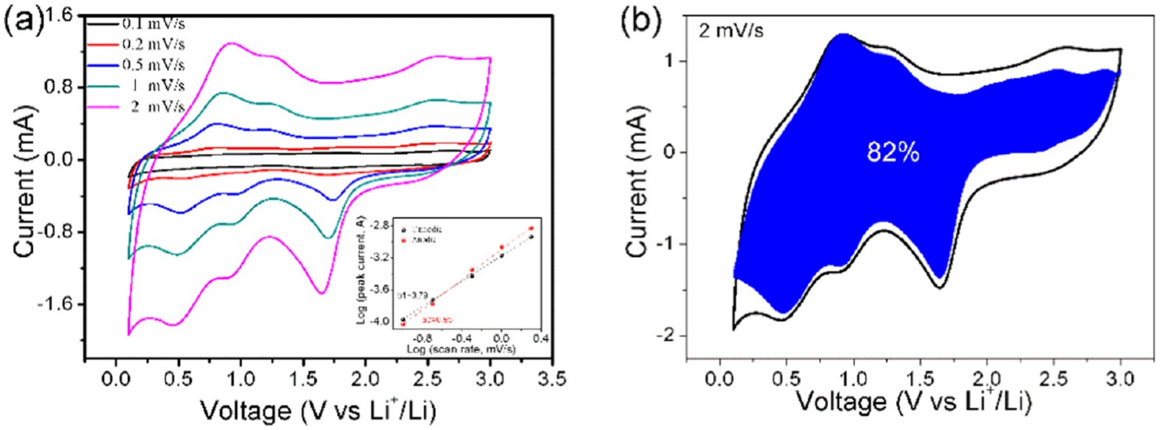

Figure 8. Quantitatively capacitive analysis of Li-ion storage behavior in VO_x-500. (a) CV curves at different scan rates and relationships between logarithm cathodic/anodic peak currents and logarithm scan rates (inset). (b) Capacitive Li-ion storage contributions at a scan rate of 2 mV/s.

The intriguing electrochemical properties of VO_x-500 material can be attributed to its unique composition and structural characteristics, as schematically shown in Figure 9: (i) the porous framework consisting of nanosized building blocks endows an enlarged electrode/electrolyte interface, featuring better electrolyte permeation, and diffusion, as well as reduced Li^+-ion diffusion path; (ii) the in situ carbon doping can boost the electrical conduction in the electrode and buffer its volume expansion during lithiation; and (iii) the coexistence of hybridized V_2O_3/VO_2 phases with self-building electric field can promote Li^+/e^- transport/transfer at the heterointerfaces. The synergy of the above features may contribute to the extrinsic pseudocapacitance-dominant Li-ion storage process in the porous hybrid electrode with superior rate property and cycle stability.

4. CONCLUSIONS

Unique porous phase-hybridized V_2O_3/VO_2 heterostructure material has been successfully fabricated via a refluxing process following annealing. Conductive carbon species are in situ incorporated into the porous framework during thermal decomposition. Owing to the integrated features of porous

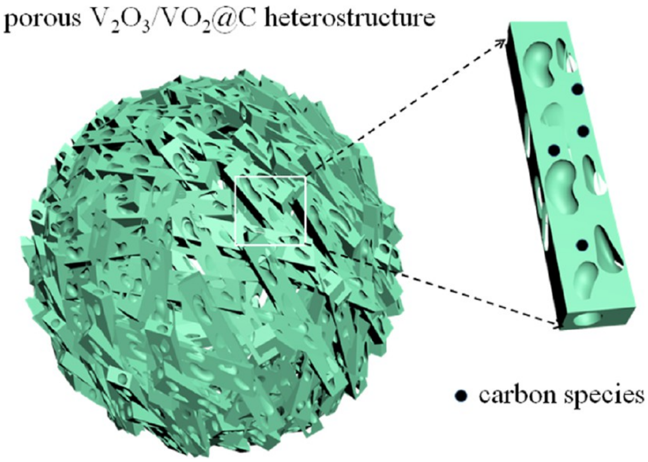

Figure 9. Schematic illustration of the structure characteristics of the porous VO_x-500 material with hybridized V_2O_3/VO_2 phases as anode in LIBs.

structures, phase hybridization and doping of conductive carbon, the resulting hybrid material exhibits superior Li-ion storage property. The current strategy may be extended to the design and synthesis of other transition-metal oxides/sulfides electrode materials for broad use in Li/Na-ion batteries and supercapacitors.

■ ASSOCIATED CONTENT

Ⓢ Supporting Information

The Supporting Information is available free of charge on the ACS Publications website at DOI: 10.1021/acsami.7b13658.

> SEM images of ammonium metavanadate (NH_4VO_3) and vanadium glycolate (VG) precursor (Figure S1); XRD patterns of vanadium oxides samples (Figure S2); TG/DSC curves of VO_x-500 sample (Figure S3); SEM images of VO_x-300 and VO_x-400 (Figure S4); SEM images of VO_x-600 and VO_x-700 (Figure S5); XRD pattern and SEM image of the sample synthesized by refluxing following annealing at 500 °C for 2 h in Ar (Figure S6) (PDF)

■ AUTHOR INFORMATION

Corresponding Authors

*E-mail: apwjzh@cityu.edu.hk (W.Z.).
*E-mail: bao-lian.su@unamur.be (B.-L.S.).
*E-mail: gzcao@u.washington.edu (G.C.).

ORCID

Hong-En Wang: 0000-0002-6859-5683
Yu Li: 0000-0002-1282-5312
Wenjun Zhang: 0000-0002-4497-0688
Guozhong Cao: 0000-0003-1498-4517

Notes

The authors declare no competing financial interest.

■ ACKNOWLEDGMENTS

This work is supported by the National Natural Science Foundation of China (51302204, 21671155, and 51472190), National Key Research and Development Program of China (2016YFA0202602), Program for Changjiang Scholars and Innovative Research Team in University (IRT_15R52), and International Science & Technology Cooperation Program of China (2015DFE52870). H.-E.W. and Y.L. acknowledge Hubei Provincial Department of Education for the "Chutian Scholar" program. H.-E.W. and X.Z. thank China Scholarship Council (CSC) for financial supports for their study in University of Washington, Seattle, WA. The authors also thank C.-Y. Zhao for kind help with additional experiments during revision stage.

■ REFERENCES

(1) Goodenough, J. B.; Park, K.-S. The Li-Ion Rechargeable Battery: A Perspective. *J. Am. Chem. Soc.* **2013**, *135*, 1167−1176.

(2) Massé, R. C.; Liu, C.; Li, Y.; Mai, L.; Cao, G. Energy storage through intercalation reactions: electrodes for rechargeable batteries. *Natl. Sci. Rev.* **2017**, *4*, 26−53.

(3) Lu, J.; Chen, Z.; Ma, Z.; Pan, F.; Curtiss, L. A.; Amine, K. The role of nanotechnology in the development of battery materials for electric vehicles. *Nat. Nanotechnol.* **2016**, *11*, 1031−1038.

(4) Xin, S.; Chang, Z.; Zhang, X.; Guo, Y.-G. Progress of rechargeable lithium metal batteries based on conversion reactions. *Natl. Sci. Rev.* **2017**, *4*, 54−70.

(5) Yu, Z.-L.; Xin, S.; You, Y.; Yu, L.; Lin, Y.; Xu, D.-W.; Qiao, C.; Huang, Z.-H.; Yang, N.; Yu, S.-H.; Goodenough, J. B. Ion-Catalyzed Synthesis of Microporous Hard Carbon Embedded with Expanded Nanographite for Enhanced Lithium/Sodium Storage. *J. Am. Chem. Soc.* **2016**, *138*, 14915−14922.

(6) Wu, H.; Cui, Y. Designing nanostructured Si anodes for high energy lithium ion batteries. *Nano Today* **2012**, *7*, 414−429.

(7) Wang, H. E.; Xi, L. J.; Ma, R. G.; Lu, Z. G.; Chung, C. Y.; Bello, I.; Zapien, J. A. Microwave-assisted hydrothermal synthesis of porous SnO_2 nanotubes and their lithium ion storage properties. *J. Solid State Chem.* **2012**, *190*, 104−110.

(8) Wang, H. E.; Lu, Z. G.; Xi, L. J.; Ma, R. G.; Wang, C. D.; Zapien, J. A.; Bello, I. Facile and Rapid Synthesis of Highly Porous Wirelike TiO_2 as Anodes for Lithium-Ion Batteries. *ACS Appl. Mater. Interfaces* **2012**, *4*, 1608−1613.

(9) Cai, Y.; Wang, H.-E.; Zhao, X.; Huang, F.; Wang, C.; Deng, Z.; Li, Y.; Cao, G.; Su, B.-L. Walnut-like Porous Core/Shell TiO_2 with Hybridized Phases Enabling Fast and Stable Lithium Storage. *ACS Appl. Mater. Interfaces* **2017**, *9*, 10652−10663.

(10) Yin, K.; Cai, Y.; Zheng, X.; Deng, Z.; Su, B.-L.; Wang, H.-E. Hierarchical porous flower-like TiO_2-B constructed by thin nanosheets for efficient lithium storage. *Mater. Lett.* **2017**, *201*, 93−96.

(11) Zhao, X.; Sui, J.; Li, F.; Fang, H.; Wang, H.; Li, J.; Cai, W.; Cao, G. Lamellar $MoSe_2$ nanosheets embedded with MoO_2 nanoparticles: novel hybrid nanostructures promoted excellent performances for lithium ion batteries. *Nanoscale* **2016**, *8*, 17902−17910.

(12) Zhao, X.; Wang, H.-E.; Massé, R. C.; Cao, J.; Sui, J.; Li, J.; Cai, W.; Cao, G. Design of coherent anode materials with 0D Ni_3S_2 nanoparticles self-assembled on 3D interconnected carbon networks for fast and reversible sodium storage. *J. Mater. Chem. A* **2017**, *5*, 7394−7402.

(13) Zhou, F.; Xin, S.; Liang, H.-W.; Song, L.-T.; Yu, S.-H. Carbon Nanofibers Decorated with Molybdenum Disulfide Nanosheets: Synergistic Lithium Storage and Enhanced Electrochemical Performance. *Angew. Chem., Int. Ed.* **2014**, *53*, 11552−11556.

(14) Shan, T.-T.; Xin, S.; You, Y.; Cong, H.-P.; Yu, S.-H.; Manthiram, A. Combining Nitrogen-Doped Graphene Sheets and MoS_2: A Unique Film-Foam-Film Structure for Enhanced Lithium Storage. *Angew. Chem., Int. Ed.* **2016**, *55*, 12783−12788.

(15) Wang, H.-E.; Zhao, X.; Li, X.; Wang, Z.; Liu, C.; Lu, Z.; Zhang, W.; Cao, G. rGO/SnS_2/TiO_2 heterostructured composite with dual-confinement for enhanced lithium-ion storage. *J. Mater. Chem. A* **2017**, *5*, 25056−25063.

(16) Wu, C.; Feng, F.; Xie, Y. Design of vanadium oxide structures with controllable electrical properties for energy applications. *Chem. Soc. Rev.* **2013**, *42*, 5157−5183.

(17) Graf, D.; Schläfer, J.; Garbe, S.; Klein, A.; Mathur, S. Interdependence of Structure, Morphology, and Phase Transitions in

CVD Grown VO_2 and V_2O_3 Nanostructures. *Chem. Mater.* **2017**, *29*, 5877−5885.

(18) Liu, P.; Zhu, K.; Gao, Y.; Luo, H.; Lu, L. Recent Progress in the Applications of Vanadium-Based Oxides on Energy Storage: from Low-Dimensional Nanomaterials Synthesis to 3D Micro/Nano-Structures and Free-Standing Electrodes Fabrication. *Adv. Energy Mater.* **2017**, No. 1700547.

(19) Wang, H.-E.; Chen, D.-S.; Cai, Y.; Zhang, R.-L.; Xu, J.-M.; Deng, Z.; Zheng, X.-F.; Li, Y.; Bello, I.; Su, B.-L. Facile synthesis of hierarchical and porous V_2O_5 microspheres as cathode materials for lithium ion batteries. *J. Colloid Interface Sci.* **2014**, *418*, 74−80.

(20) Liu, H.; Wang, Y.; Li, H.; Yang, W.; Zhou, H. Flowerlike Vanadium Sesquioxide: Solvothermal Preparation and Electrochemical Properties. *ChemPhysChem* **2010**, *11*, 3273−3280.

(21) Yan, B.; Li, X.; Bai, Z.; Lin, L.; Chen, G.; Song, X.; Xiong, D.; Li, D.; Sun, X. Superior sodium storage of novel VO_2 nano-microspheres encapsulated into crumpled reduced graphene oxide. *J. Mater. Chem. A* **2017**, *5*, 4850−4860.

(22) An, X.; Yang, H.; Wang, Y.; Tang, Y.; Liang, S.; Pan, A.; Cao, G. Hydrothermal synthesis of coherent porous V_2O_3/carbon nanocomposites for high-performance lithium- and sodium-ion batteries. *Sci. China Mater.* **2017**, *60*, 717−727.

(23) Liu, X.; Liu, R.; Zeng, L.; Huang, X.; Chen, X.; Zheng, C.; Xu, Y.; Qian, Q.; Wei, M.; Chen, Q. Facile preparation of a V_2O_3/carbon fiber composite and its application for long-term performance lithium-ion batteries. *New J. Chem.* **2017**, *41*, 5380−5386.

(24) McNulty, D.; Buckley, D. N.; O'Dwyer, C. V_2O_3 Polycrystalline Nanorod Cathode Materials for Li-Ion Batteries with Long Cycle Life and High Capacity Retention. *ChemElectroChem* **2017**, *4*, 2037−2044.

(25) Mai, L.; Wei, Q.; An, Q.; Tian, X.; Zhao, Y.; Xu, X.; Xu, L.; Chang, L.; Zhang, Q. Nanoscroll Buffered Hybrid Nanostructural VO_2(B) Cathodes for High-Rate and Long-Life Lithium Storage. *Adv. Mater.* **2013**, *25*, 2969−2973.

(26) Niu, C.; Meng, J.; Han, C.; Zhao, K.; Yan, M.; Mai, L. VO_2 Nanowires Assembled into Hollow Microspheres for High-Rate and Long-Life Lithium Batteries. *Nano Lett.* **2014**, *14*, 2873−2878.

(27) Ren, G.; Hoque, M. N. F.; Pan, X.; Warzywoda, J.; Fan, Z. Vertically aligned VO_2(B) nanobelt forest and its three-dimensional structure on oriented graphene for energy storage. *J. Mater. Chem. A* **2015**, *3*, 10787−10794.

(28) Liu, P.; Xu, Y.; Zhu, K.; Bian, K.; Wang, J.; Sun, X.; Gao, Y.; Luo, H.; Lu, L.; Liu, J. Ultrathin VO_2 nanosheets self-assembled into 3D micro/nano-structured hierarchical porous sponge-like micro-bundles for long-life and high-rate Li-ion batteries. *J. Mater. Chem. A* **2017**, *5*, 8307−8316.

(29) Wei, Q.; Xiong, F.; Tan, S.; Huang, L.; Lan, E. H.; Dunn, B.; Mai, L. Porous One-Dimensional Nanomaterials: Design, Fabrication and Applications in Electrochemical Energy Storage. *Adv. Mater.* **2017**, *29*, No. 1602300.

(30) Xi, L. J.; Wang, H.-E.; Lu, Z. G.; Yang, S. L.; Ma, R. G.; Deng, J. Q.; Chung, C. Y. Facile synthesis of porous $LiMn_2O_4$ spheres as positive electrode for high-power lithium ion batteries. *J. Power Sources* **2012**, *198*, 251−257.

(31) Wang, H.-E.; Qian, D.; Lu, Z.-g.; Li, Y.-k. Synthesis and electrochemical properties of $LiMn_2O_4$ and $LiCoO_2$-coated $LiMn_2O_4$ cathode materials. *J. Alloys Compd.* **2012**, *517*, 186−191.

(32) Wang, H.-E.; Cheng, H.; Liu, C.; Chen, X.; Jiang, Q.; Lu, Z.; Li, Y. Y.; Chung, C. Y.; Zhang, W.; Zapien, J. A.; Martinu, L.; Bello, I. Facile synthesis and electrochemical characterization of porous and dense TiO_2 nanospheres for lithium-ion battery applications. *J. Power Sources* **2011**, *196*, 6394−6399.

(33) Wang, H.-E.; Jin, J.; Cai, Y.; Xu, J.-M.; Chen, D.-S.; Zheng, X.-F.; Deng, Z.; Li, Y.; Bello, I.; Su, B.-L. Facile and fast synthesis of porous TiO_2 spheres for use in lithium ion batteries. *J. Colloid Interface Sci.* **2014**, *417*, 144−151.

(34) Pan, A.; Wu, H. B.; Yu, L.; Lou, X. W. D. Template-Free Synthesis of VO_2 Hollow Microspheres with Various Interiors and Their Conversion into V_2O_5 for Lithium-Ion Batteries. *Angew. Chem., Int. Ed.* **2013**, *52*, 2226−2230.

(35) Wang, J.; Tang, H.; Zhang, L.; Ren, H.; Yu, R.; Jin, Q.; Qi, J.; Mao, D.; Yang, M.; Wang, Y.; Liu, P.; Zhang, Y.; Wen, Y.; Gu, L.; Ma, G.; Su, Z.; Tang, Z.; Zhao, H.; Wang, D. Multi-shelled metal oxides prepared via an anion-adsorption mechanism for lithium-ion batteries. *Nat. Energy* **2016**, *1*, No. 16050.

(36) Zeng, L.; Zheng, C.; Xi, J.; Fei, H.; Wei, M. Composites of V_2O_3-ordered mesoporous carbon as anode materials for lithium-ion batteries. *Carbon* **2013**, *62*, 382−388.

(37) Li, X.; Fu, J.; Pan, Z.; Su, J.; Xu, J.; Gao, B.; Peng, X.; Wang, L.; Zhang, X.; Chu, P. K. Peapod-like V_2O_3 nanorods encapsulated into carbon as binder-free and flexible electrodes in lithium-ion batteries. *J. Power Sources* **2016**, *331*, 58−66.

(38) Shi, Y.; Chou, S.-L.; Wang, J.-Z.; Li, H.-J.; Liu, H.-K.; Wu, Y.-P. In-situ hydrothermal synthesis of graphene woven VO_2 nanoribbons with improved cycling performance. *J. Power Sources* **2013**, *244*, 684−689.

(39) Weeks, C.; Song, Y.; Suzuki, M.; Chernova, N. A.; Zavalij, P. Y.; Whittingham, M. S. The one dimensional chain structures of vanadyl glycolate and vanadyl acetate. *J. Mater. Chem.* **2003**, *13*, 1420−1423.

(40) Ragupathy, P.; Shivakumara, S.; Vasan, H. N.; Munichandraiah, N. Preparation of Nanostrip V_2O_5 by the Polyol Method and Its Electrochemical Characterization as Cathode Material for Rechargeable Lithium Batteries. *J. Phys. Chem. C* **2008**, *112*, 16700−16707.

(41) Bergerud, A.; Buonsanti, R.; Jordan-Sweet, J. L.; Milliron, D. J. Synthesis and Phase Stability of Metastable Bixbyite V_2O_3 Colloidal Nanocrystals. *Chem. Mater.* **2013**, *25*, 3172−3179.

(42) Moatti, A.; Sachan, R.; Prater, J.; Narayan, J. Control of Structural and Electrical Transitions of VO_2 Thin Films. *ACS Appl. Mater. Interfaces* **2017**, *9*, 24298−24307.

(43) Zheng, Y.; Zhou, T.; Zhang, C.; Mao, J.; Liu, H.; Guo, Z. Boosted Charge Transfer in SnS/SnO_2 Heterostructures: Toward High Rate Capability for Sodium-Ion Batteries. *Angew. Chem., Int. Ed.* **2016**, *55*, 3408−3413.

(44) Biesinger, M. C.; Lau, L. W. M.; Gerson, A. R.; Smart, R. S. C. Resolving surface chemical states in XPS analysis of first row transition metals, oxides and hydroxides: Sc, Ti, V, Cu and Zn. *Appl. Surf. Sci.* **2010**, *257*, 887−898.

(45) Jiang, L.; Qu, Y.; Ren, Z.; Yu, P.; Zhao, D.; Zhou, W.; Wang, L.; Fu, H. In Situ Carbon-Coated Yolk−Shell V_2O_3 Microspheres for Lithium-Ion Batteries. *ACS Appl. Mater. Interfaces* **2015**, *7*, 1595−1601.

(46) Song, H. J.; Choi, M.; Kim, J.-C.; Park, S.; Lee, C. W.; Hong, S.-H.; Kim, D.-W. Li-electroactivity of thermally-reduced V_2O_3 nanoparticles. *Mater. Lett.* **2016**, *180*, 243−246.

(47) Shi, Y.; Zhang, Z.; Wexler, D.; Chou, S.; Gao, J.; Abruña, H. D.; Li, H.; Liu, H.; Wu, Y.; Wang, J. Facile synthesis of porous V_2O_3/C composites as lithium storage material with enhanced capacity and good rate capability. *J. Power Sources* **2015**, *275*, 392−398.

(48) Chao, D.; Zhu, C.; Xia, X.; Liu, J.; Zhang, X.; Wang, J.; Liang, P.; Lin, J.; Zhang, H.; Shen, Z. X.; Fan, H. J. Graphene Quantum Dots Coated VO_2 Arrays for Highly Durable Electrodes for Li and Na Ion Batteries. *Nano Lett.* **2015**, *15*, 565−573.

(49) Huang, S.-Z.; Cai, Y.; Jin, J.; Li, Y.; Zheng, X.-F.; Wang, H.-E.; Wu, M.; Chen, L.-H.; Su, B.-L. Annealed vanadium oxide nanowires and nanotubes as high performance cathode materials for lithium ion batteries. *J. Mater. Chem. A* **2014**, *2*, 14099−14108.

(50) Augustyn, V.; Simon, P.; Dunn, B. Pseudocapacitive oxide materials for high-rate electrochemical energy storage. *Energy Environ. Sci.* **2014**, *7*, 1597−1614.

(51) Jafari, S. M.; Khosravi, M.; Mollazadeh, M. Nanoporous hard carbon microspheres as anode active material of lithium ion battery. *Electrochim. Acta* **2016**, *203*, 9−20.

DOI: 10.1021/acsami.7b13658
ACS Appl. Mater. Interfaces 2017, 9, 43665−43673